Design of a Resonant Plate for Pyroshock Testing based on Shape and Size Heuristic Optimization

Luca VIALE[1], Alessandro Paolo DAGA[1], Luigi GARIBALDI[1]

[1]Department of Mechanical and Aerospace Engineering, Politecnico di Torino,
Corso Duca degli Abruzzi 24, 10129 Torino, Italy
luca.viale@polito.it

Abstract

Resonant plate testing is a common laboratory test method for qualifying space equipment which needs to withstand strong high-frequency shocks, usually activated by pyrotechnic devices and transmitted to the structure. Given their impulsive nature, shocks could critically damage onboard equipment and jeopardize the success of the mission. NASA-STD-7003A international standards are usually adopted to establish the requirements, in terms of a Shock Response Spectrum (SRS), for the qualification of space equipment according to the launch vehicle characteristics. To foster repeatability and safety in laboratories, the most common test facilities exploit the launch of an impacting object (e.g., hammers, dropping masses, pistons, or bullets) on a resonant plate on which the component under test is mounted. In this work, a numerical model able to completely simulate a pyroshock test is used to perform a shape and size heuristic optimization of a resonant plate to match the required SRS. Limiting the energy inputs, the performances of regular polygonal rather than irregular quadrilateral shapes and sizes are investigated and compared. The algorithm features an embedded Computer-Aided Design (CAD) modeler, a Finite Element (FE) solver, and a Genetic Algorithm (GA) optimizer, ensuring accuracy and flexibility in predicting the behavior of a resonant plate with a complex shape. The optimized design of a resonant plate permits improvements in both the SRS accuracy and the time and cost efficiency of its tuning.

1 Introduction

When dealing with space and aerospace equipment, international standards require the manufacturers to test their ability to withstand the strong excitations produced during the launch. In fact, structural subsystems of the rockets are commonly released by explosive charges of pyrotechnic nature, producing strong shocks. The important impulsive nature of such “pyroshocks” (as are commonly referred to) produces transient structural responses whose intensity could easily damage the carried equipment in the vicinity of the energy release zone. Hence, the mechanical resistance of these equipment must be tested experimentally as prescribed by standards such as the NASA 7003 [1], the MIL-STD-810F, Method 517 [2], the IEST RP Pyroshock Testing Technique [3] and the ESA ECSS experimental standard [4]. In these documents, a Shock Response Spectrum (SRS) is usually defined as a testing requirement, as the SRS provides a measure of the damage-ability of the pyroshock [5,6]. Also, many testing procedures for emulating the effect of a pyroshock in a more controlled and safer environment are described. Among the others, one of the most effective and widely used is the resonant plate pyroshock testing [7,8]. The object under test is mounted on one side of a huge metal plate, which is hit by a impacting object (e.g., a dropping mass, a pendulum, a projectile, a hammer, a piston, etc.), providing the energy necessary to excite the item within the SRS requirement range. In this regard, despite remaining the standard requirement (see [9] for other possible alternatives), the SRS lacks intuitiveness, as many different combinations of testing parameters can produce similar curves. That’s why the effect of the main test parameters was experimentally explored over the years, as in [10,11], where the plate constraint conditions, the impacting body material and geometry, the impact velocity and location

and the anvil plate material were studied. At the same time, numerical models were also used so as to simulate the contact and the produced pyroshock based on NASTRAN and DYTRAN models (see [12]). Different from these Finite Element Analysis (FEA) tools, but sharing the same computational complexity, Statistical Energy Analysis (SEA) methods can be used [13,14], as well as Transient Statistical Energy Analysis (TSEA) [15,16], which can be even combined in Virtual Mode Synthesis and Simulation (VMSS) [17] or with FEA, as proposed in [18,19].

Unfortunately, such Advanced Models are too complex and computationally expensive to be used to automate the test parameters selection. In this respect, papers [20,21] proposed a simpler way to numerically simulate the behavior of the plate exploiting a simplified m-dof model, with lumped masses and stiffnesses, and a Frequency Domain Convolutional scheme, allowing a quick and reliable tuning of all the main test variables.

In this work, the m-dof simplified model is substituted by a more advanced FE model (FEM), which improves the results accuracy at the cost of slightly larger computational times. Being the computational burden not too high anyway (as the contact is not accounted in the FEM), this enables to set a heuristic optimization of the shape and size of the plate, which can be automatically designed by the algorithm minimizing the distance of the simulated SRS from the requirement. The complete model description is given in Section 2. The optimization results are reported and discussed in Section 3, while final conclusions will be derived in Section 4.

2 Methodology

The proposed approach is meant to provide a reasonably fast yet accurate model for simulating the resulting SRS generated by a shock due to the hit of a projectile on the base plate. The idea is that of decomposing the physical model, as depicted in Figure 1, into 3 sub-models:

1. A FEM model of a plate able to compute the point inertance of a metal plate of any shape and material;
2. A numerical model for the impact, defining the input pulse signal as a function of the contact materials and projectile momentum in terms of mass and speed;
3. A numerical model for computing the maximax SRS with a Q factor of 10, i.e., the maximum of the absolute value of the time acceleration of the (negligible) mass of an equivalent, calibrated s-dof mounted on the plate with a damping factor of 5% (and iterated while increasing the natural frequency of the s-dof to cover the entire range of frequency of interest, commonly from 100 to 10.000 Hz)

The three sub-models are then merged by a Frequency Domain Convolutional scheme so as to speed up the procedure. From a practical point of view, the Convolution Theorem of the Fourier Transform is exploited, so as to produce the final equation:

$$\ddot{X}_{SRS}^{\Omega_c}(\omega) = F_j(\omega) \cdot I_{jk}(\omega) \cdot T_{SRS}^{\Omega_c}(\omega) \tag{1}$$

Given the spectrum of the input impact force $F_i(\omega)$, then, and multiplying it by the Inertance $I_{ik}(\omega)$ and by the Transmissibility of a s-dof $T_{SRS}^{\Omega_c}(\omega)$ it is possible to directly find the corresponding $SRS(\Omega_c)$ as:

$$SRS(\Omega_c) = \max\left(\text{abs}\left(\ddot{x}_{SRS}^{\Omega_c}(t)\right)\right) \tag{2}$$

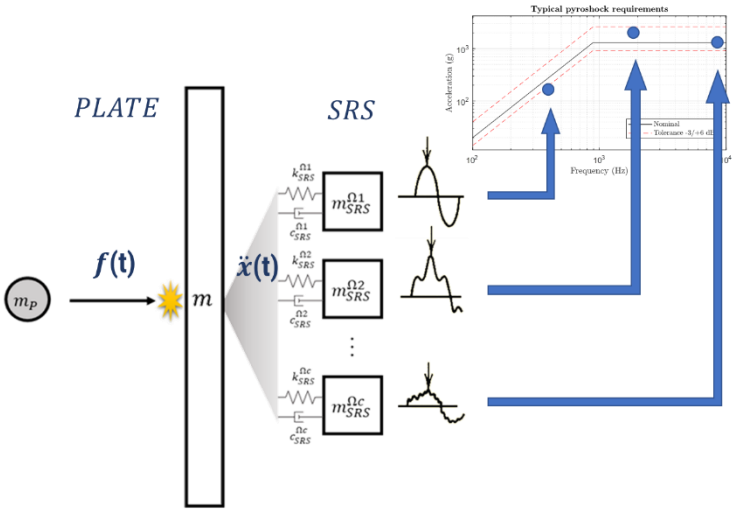

Figure 1: A scheme of the physical model.

The single sub-models are described in the following sub-sections.

2.1 Numerical Model of a resonant plate Pyroshock test (FEM)

In this work, the FEM model of the resonant fixture is innovatively solved in Matlab. To cope with the need of automation, the size and geometry of the plate are directly governed by the software by integrating OpenSCAD [22] as a 3D modeller. By setting free-free boundary conditions and selecting the centre of the plate as input force application point and acceleration measurement point, a discrete estimate of the point inertance $I_{ij}(\omega)$ can be obtained by the software at a desired frequency resolution, in a desired range.

Being the scope of this work the design of the shape and size of the plate provided a requirement, it was decided to test the family of shapes defined by regular n-sided polygons, i.e., equilateral and equiangular shapes defined by the number of sides n and the radius of the circumscribed circle R.

A summary of all the relevant parameters for the plate FEM is reported in Figure 2 and Table 1.

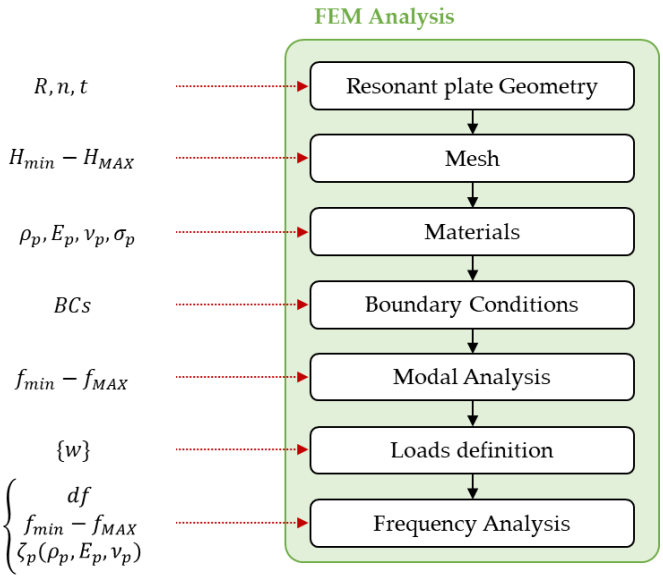

Figure 2: Block scheme for the FEM analysis and the useful parameters.

Parameter Name	Parameter Description
R	Radius of the circumscribed circle
n	Number of sides of the polygon
t	Thickness of the plate
$H_{min} - H_{max}$	Mesh size - range
ρ_p	Density of the plate material
E_p	Young's modulus of the plate material
ν_p	Poisson's ratio of the plate material
σ_p	Yield stress of the plate material
BC_s	Type of Boundary conditions
$f_{min} - f_{max}$	Range of frequency for the study
$\{w\}$	Input Force intensity and direction
df	Frequency resolution for the Inertance
ζ_p	Modal damping factor of the plate

Table 1: FEM model Parameters Description.

2.2 Input force (Pulse) Definition

In this work, the impact force $f(t)$ is modelled by two half windows (left and right) whose shape is defined as half a raised cosine (i.e., the von Hann window). The total time duration τ (as shown in Figure 3) is estimated by Hertzian contact theory as a function of the projectile geometric parameters m_s, v_s and R_s, respectively the mass, the velocity and the contact radius of the bullet and the bullet-plate contact materials. The exploited equation [23] is here reported:

$$\tau = 2{,}9432 \cdot \left[\frac{15 m_s \left(\frac{1-\nu_s^2}{E_s} + \frac{1-\nu_p^2}{E_p} \right)}{16\sqrt{R_s \nu_s}} \right]^{2/5} \tag{3}$$

This total time is divided into a left and a right time (i.e., τ_L and τ_R) by considering the Weir-Tallon's coefficient of restitution e [24]:

$$e = \frac{\tau_R}{\tau_L} = \frac{3{,}1}{\rho_s^{1/8}\sqrt{E_c}} \left[\frac{\min(\sigma_s, \sigma_p)^5}{\nu_s^2} \right]^{1/8} \tag{4}$$

Finally, to simplify the computation, the total integral is normalized to the unit area to produce a $f_0(t)$, and the momentum is left as a multiplier (see eq. 5). $f_0(t)$ is sampled in the time domain and the Fast Fourier Transform (FFT) is used to derive $F_i(\omega)$.

$$F_j(t) = m_s v_s (1+e) F_0(t) \tag{5}$$

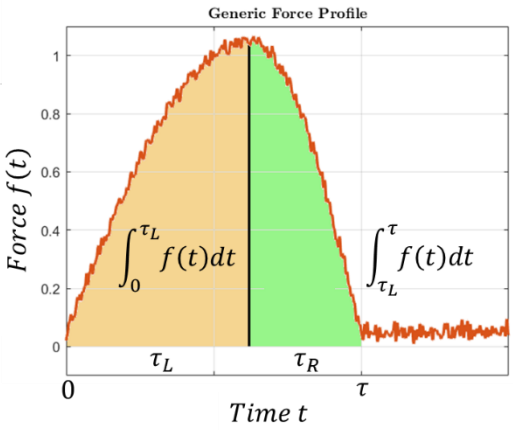

Figure 3: Definition of the relevant impulse parameters.

A summary of all the relevant parameters for the input pulse signal is reported in Figure 4 and Table 2.

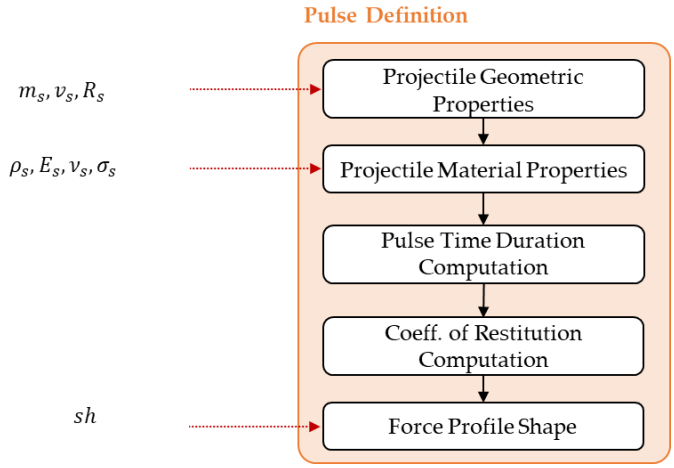

Figure 4: Definition of the pulse numerical model parameters.

Parameter Name	Parameter Description
m_s	Bullet mass
v_s	Bullet speed
R_s	Bullet contact radius
ρ_s	Density of the plate material
E_s	Young's modulus of the bullet
ν_s	Poisson's ratio of the bullet
sh	Window shape (von Hann window)

Table 2: Pulse numerical model parameters.

2.3 SRS Definition

The maximax SRS with a Q factor of 10 is finally evaluated from the acceleration of the equivalent, calibrated single degree of freedom (s-dof) system. This is obtained in the Frequency Domain as a product by a well-known FRF called Transmissibility [25], defined as:

$$T_{SRS}^{\Omega_c}(\omega) = \frac{1 + 2r\zeta_{SRS}i}{1 - r^2 + 2r\zeta_{SRS}i} \tag{6}$$

where i is the imaginary unit, $\zeta_{SRS} = 0{,}05$ is the damping factor and r is the adimensional normalized frequency ω/Ω_c.

Iterating the computation while increasing the natural frequency Ω_c of the s-dof with steps of $1/24$ of octave, the entire range of frequency of interest from 100 to 10.000 Hz can be covered, so that eq. (2) can finally be used to find the resulting SRS, to be compared to the requirement.

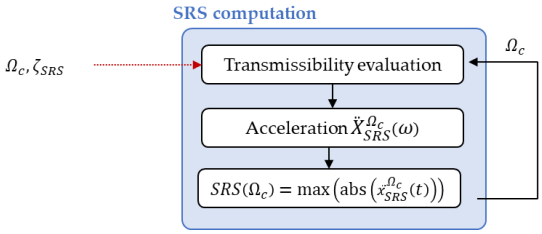

Figure 5: Definition of the SRS computation parameters.

2.4 Genetic Algorithm Shape and Size Optimization

The frequency model just described makes it possible to predict the SRS with good precision as the operating conditions vary. In fact, the numerous parameters introduced guarantee the high flexibility of the model. Among these, the geometric parameters are usually fixed since the plate geometry does not vary and the objective is to determine the appropriate momentum to meet the shock test requirements. However, the present model can be extended to solve the inverse problem, i.e. optimizing the resonant plate provided the requirements.

In the literature, most of the test facilities for shock tests use a squared or - in general - quadrangular resonant plate. For instance, in [10] and in [26] two square aluminum alloy plates are used with dimensions equal to 1x1x0.03 m^3 and 1x1x0.05 m^3, respectively. In [27] a rectangular plate with dimensions 1.2x0.5x0.03m^3 is analyzed.

The goal of this work is to investigate how the shape and size of the resonant plate affect the SRS profiles. In particular, the optimal plate is searched using a Genetic Algorithm. The implementation of an embedded Computer-Aided Design (CAD) modeler and a Finite Element (FE) solver allows the prediction of the behavior of a resonant plate with a complex and variable shape.

The model has been set up in such a way that the plate geometry is defined on the basis of three parameters: the circumscribed radius r_p to the regular geometry of the plate, the number of sides n_p of the defined polygon, and the plate thickness z_p. Thanks to these parameters it is possible to investigate the behavior of plates with variable shape and size. Furthermore, since the mass of the plate is proportional to its size, the mass m_s and velocity v_s of the impacting object have also been optimized. In fact, more massive plates need higher momentum and vice versa. In this way, it is possible to optimize the SRS profile independent of other confounding factors. All these parameters have been discretized in specific ranges to avoid local minima problems typical of heuristic optimizers.

It is finally necessary to define a score function to solve the minimization problem. Among the most used evaluation criteria, the Root Mean Square Error (RMSE) and the Mean Absolute Error (MAE) could be found. However, the score function has been determined according to this specific case. Given that pyroshock requirements are usually established with the related tolerances, the score function is adapted to evaluate the error only when the SRS falls outside the tolerances region. In addition, the score function should also take into account the fact that undertesting conditions are more critical than the overtesting ones. For all these reasons, the score function adopted in the present work has been defines as reported in Eq. (1).

$$score_{GA} = \begin{cases} log_{10}\left(\frac{\ddot{x}_{SRS}(\Omega_c)}{\ddot{x}_{req}(\Omega_c)}\right)^{log_{10}\left(\frac{\ddot{x}^{+}_{tol}(\Omega_c)}{\ddot{x}_{SRS}(\Omega_c)}\right)} & if\ \ddot{x}_{SRS}(\Omega_c) > \ddot{x}^{+}_{tol}(\Omega_c) \\ 0 & if\ \ddot{x}^{-}_{tol}(\Omega_c) < \ddot{x}_{SRS}(\Omega_c) < \ddot{x}^{+}_{tol}(\Omega_c) \\ log_{10}\left(\frac{\ddot{x}_{SRS}(\Omega_c)}{\ddot{x}_{req}(\Omega_c)}\right)^{log_{10}\left(\frac{\ddot{x}^{-}_{tol}(\Omega_c)}{\ddot{x}_{SRS}(\Omega_c)}\right)} & if\ \ddot{x}_{SRS}(\Omega_c) < \ddot{x}^{-}_{tol}(\Omega_c) \end{cases} \quad (7)$$

where $\ddot{x}_{SRS}(\Omega_c)$ is the calculated value of the acceleration synchronized to the resonant frequency Ω_c of the c-th s-dof system for the SRS calculation, $\ddot{x}_r(\Omega_c)$ is the test requirement (or the generic reference curve) in terms of SRS acceleration, $\ddot{x}^{-}_{tol}$ and $\ddot{x}^{+}_{tol}$ are respectively the values of the lower and upper tolerances. For the sake of clarity, Figure 6 shows the colormap representing the score applied to the SRS predictions, considering a standard requirement.

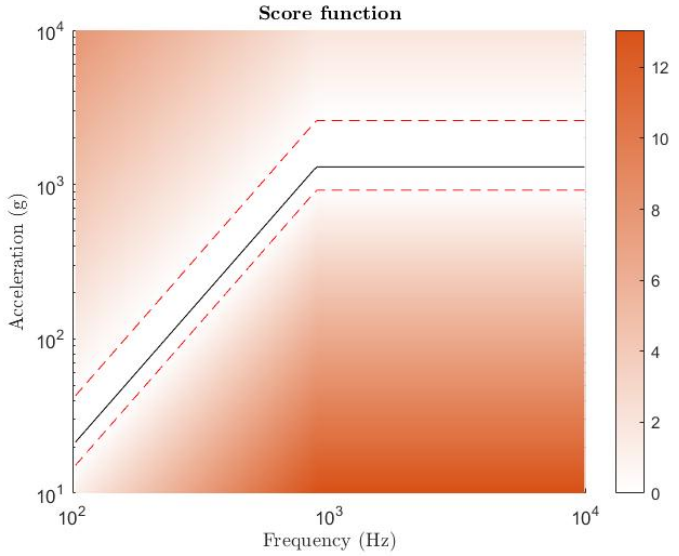

Figure 6: Colormap describing the adopted score function according to the specified requirements and the related tolerances.

3 Results and Discussion

The shape and size optimization of the resonant plate has been obtained by minimizing the cost function in a discrete multidimensional space. This multivariate space is generated by the five parameters previously defined, which are summarized in Table 3. The upper and lower bounds were established based on typical applications, ensuring consistency between parameters. Similarly, discretization was established considering the best trade-off between the total number of combinations and the computational burden. The number of sides n_p of the polygon has been set in order to consider all the regular shapes from $n_p = 3$ (triangular case) up to $n_p = 8$ (octagonal case) and, in addition, $n_p = 100$ to simulate a circular plate.

Parameter	Lower Bound	Discretization	Upper Bound
r_p	0.45 m	0.05 m	0.60 m
z_p	0.02 m	0.01 m	0.05 m
n_p	3 sides	1 side	8 sides + circle
m_s	1 kg	1 kg	10 kg
v_s	1 m/s	1 m/s	10 m/s

Table 3: Discretization of the parameters optimized by GA.

Given that the total number of possible combinations is equal to 11200 cases, the size of the population used to seed the genetic algorithm has been set equal to 50, while the number of iterations has been fixed equal to 10 to ensure the convergence of the algorithm and – at the same time – reduce the running time. GA found the best configuration as a triangular plate (n_p = 3) inscribed in a circle with radius r_p = 0.6 m and thickness z_p = 0.04 m, hit by an impacting object with mass m_s = 9 kg and velocity v_s = 1 m/s. All the other parameters present in the model have been established based on design decisions and are reported in Table 4. Figure 7 shows the optimized plate geometry with vectors indicating the input and output directions fixed in the model.

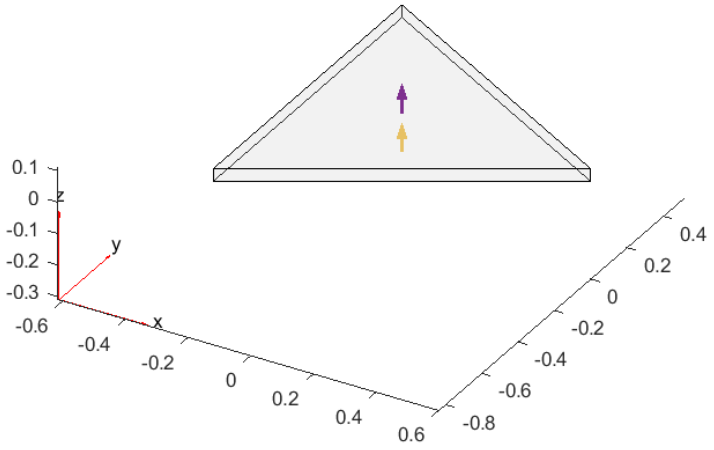

Figure 7. Shape and size optimized resonant plate.

Parameter	Value
r_p*	0.60 m
z_p*	0.04 m
n_p*	3 sides
m_s*	9 kg
v_s*	1 m/s
Plate material	Al6082
Impact location	Center of mass (0 m; 0 m)
Measurement location	Center of mass (0 m; 0 m)
Boundary conditions	Free
Impacting object material	SS303
Impacting object curvature	0.2 m
Force profile shape	von Hann window

Table 4: Fixed and optimized (indicated by the superscript *) parameters adopted to simulate the optimal configuration.

The simulation of the optimized resonant plate in the described operating conditions led to the SRS prediction shown in Figure 8. It is worth noting that the required tolerances are almost totally accomplished, and the results prove to be satisfactory.

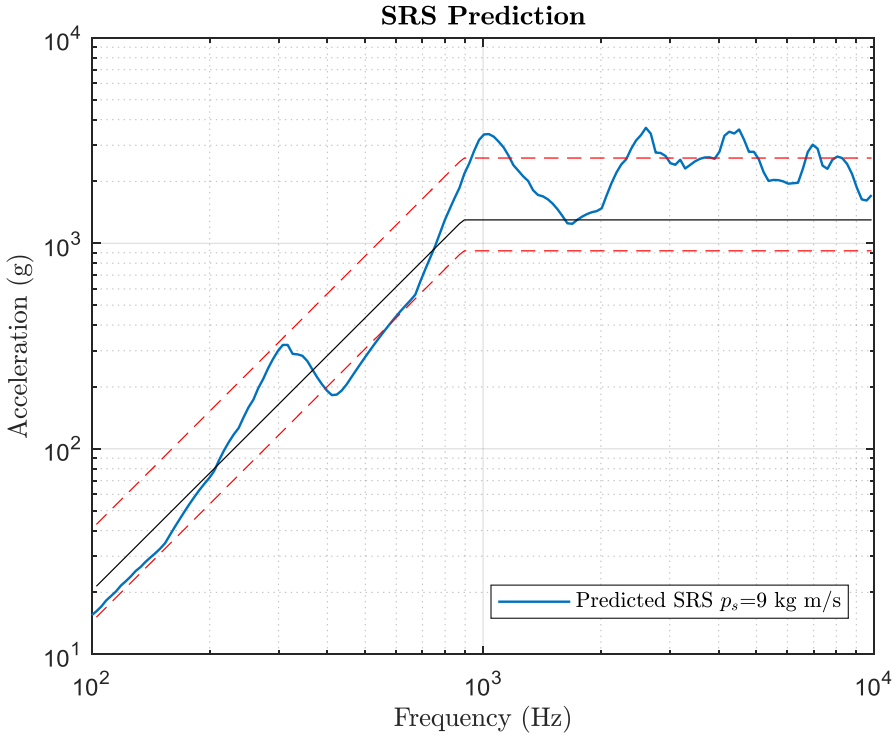

Figure 8. Simulated SRS inherent to the GA-optimized resonant plate.

4 Conclusions

The proposed work presents a numerical model able to completely simulate a pyroshock test exploiting an embedded CAD modeler and a FE solver. The model flexibility and accuracy allow to perform a shape and size GA optimization of a resonant plate to match the required SRS. The proposed results showed that a triangular plate inscribed in a circle with radius r_p = 0.6 m and thickness z_p = 0.04 m – hit by an impacting object with mass m_s = 9 kg and velocity v_s = 1 m/s – is the configuration that best meets the requirements. The predicted SRS faithfully satisfies the requirements and the related tolerances. The obtained results permit improvements in both the SRS accuracy and the time and cost efficiency of its tuning.

Nevertheless, it is necessary to remember that simplifications have been applied to reduce the model complexity and the computing time. In fact, the anvil plate and the object under test have been neglected by the geometry. These aspects require specific attention and, therefore, have been analysed in [28].

References

[1] H. Himelblau, Pyroshock Test Criteria, NASA-STD-7003A, 2011.
[2] MIL-STD-810F, Dep. Def. Test Method Stand. Environ. Eng. Consid. Lab. Tests Version F US Gov. Print. Off. (2000).
[3] A.P. One, Pyroshock Testing Techniques, (2009).
[4] E.S.A. ECSSSecretariat, R. ESTEC, ECSS-E-ST-10-03C, Space Eng.-Test. ESA Publ. Div. Noordwijk Neth. (2012).
[5] C.M. Harris, A.G. Piersol, Harris' shock and vibration handbook, McGraw-Hill New York, 2002.
[6] A. Calvi, G. Aglietti, J. Albus, M. Bellini, D. Burtin, E. Cavro, J. Dupré, C. Fabriés, S. Fransen, D. Gangloff, A. Girard, N. Gualtieri, A. Itta, G. Kerschen, W. Konrad, R. Morisset, P. Nali, A. Newerla, G. Quagliotti, A. Rittweger, N. Roy, G. Sinnema, R. Ullio, J. Vergniaud, R. Veul, J. Wijker, ECSS-E-HB-32-26A Spacecraft Mechanical Loads Analysis Handbook, Undefined. (2013).
[7] J.-R. Lee, C.C. Chia, C.-W. Kong, Review of pyroshock wave measurement and simulation for space systems, Measurement. 45 (2012) 631–642. https://doi.org/10.1016/j.measurement.2011.12.011.

[8] Y. Yan, Q.M. Li, A pyroshock signal characterization method based on shock-waveform dictionary, Int. J. Mech. Sci. 249 (2023) 108251.
[9] C. Sisemore, Defining Resonant Plate Shock Test Specifications in the Time Domain., Sandia National Lab.(SNL-NM), Albuquerque, NM (United States), 2019.
[10] M. Jonsson, Development of a shock test facility for qualification of space equipment, Dep. Appl. Mech. Göteb. Swed. (2012).
[11] C. Sisemore, M.A. Spletzer, Design of a Resonant Plate Shock Fixture to Attenuate Excessive High-Frequency Energy Inputs., Sandia National Lab.(SNL-NM), Albuquerque, NM (United States), 2017.
[12] S. Kiryenko, G. Piret, J. Kasper, ESA/ESTEC shock bench presentation, in: Spacecr. Struct. Mater. Mech. Test. 2005, 2005.
[13] F.J. Fahy, Statistical energy analysis: a critical overview, Philos. Trans. R. Soc. Lond. Ser. Phys. Eng. Sci. 346 (1994) 431–447.
[14] C.B. Burroughs, R.W. Fischer, F.R. Kern, An introduction to statistical energy analysis, J. Acoust. Soc. Am. 101 (1997) 1779–1789.
[15] R.J. Pinnington, D. Lednik, Transient statistical energy analysis of an impulsively excited two oscillator system, J. Sound Vib. 189 (1996) 249–264.
[16] B.Y. Mao, S.L. Xie, M.L. Xu, X.N. Zhang, G.H. Zhang, Simulated and experimental studies on identification of impact load with the transient statistical energy analysis method, Mech. Syst. Signal Process. 46 (2014) 307–324.
[17] E. Dalton, B. Chambers, I.I. Chambers, Analysis and validation testing of impulsive load response in complex, multi-compartmented structures, in: 36th Struct. Struct. Dyn. Mater. Conf., 1995: p. 1243.
[18] R. Ullio, P.C. Marucchi-Chierro, A. Spazio, Utilization of prediction methods in the shock environment evaluation, in: Spacecr. Struct. Mater. Mech. Test., 2001: p. 239.
[19] X. Wang, W. Liu, J. Ding, Y. Sun, Y. Dang, Pyroshock Response Prediction of Spacecraft Structure in Wide Frequency Domain Based on Acceleration FRF, Aerospace. 9 (2022) 54.
[20] L. Viale, A.P. Daga, L. Garibaldi, A. Fasana, Numerical Modeling of a Pyroshock Test Plate for Qualification of Space Equipment, in: P. Rizzo, A. Milazzo (Eds.), Eur. Workshop Struct. Health Monit., Springer International Publishing, Cham, 2023: pp. 990–999. https://doi.org/10.1007/978-3-031-07322-9_100.
[21] D. Alessandro Paolo, V. Luca, G. Luigi, F. Alessandro, M. Stefano, Frequency Domain Convolutional Model of a Pyroshock Plate for Qualification of Space Equipment, IC-MSQUARE-2022 AIP Conf. Proc. Vol. 2872. (2022).
[22] OpenSCAD, (n.d.). https://openscad.org (accessed July 22, 2022).
[23] D. Gugan, Inelastic collision and the Hertz theory of impact, Am. J. Phys. 68 (2000) 920–924.
[24] G. Weir, S. Tallon, The coefficient of restitution for normal incident, low velocity particle impacts, Chem. Eng. Sci. 60 (2005) 3637–3647.
[25] A. Fasana, S. Marchesiello, Meccanica delle vibrazioni, Clut, 2006.
[26] B.-S. Kim, J. Lee, Development of Impact Test Device for Pyroshock Simulation Using Impact Analysis, Aerospace. 9 (2022) 407.
[27] O.M.F. Morais, C.M.A. Vasques, Shock environment design for space equipment testing, Proc. Inst. Mech. Eng. Part G J. Aerosp. Eng. 231 (2017) 1154–1167.
[28] A.P. Daga, L. Viale, A. Fasana, Optimization of the Energy Input and Output Parameters for Pyroshock Testing, Survishno 2023 Conf. Proc. (2023).